Geophysical Journal International

Geophys. J. Int. (2010) **180,** 1253–1264 doi: 10.1111/j.1365-246X.2009.04474.x

Serpentinization in the trench-outer rise region offshore of Nicaragua: constraints from seismic refraction and wide-angle data

Monika Ivandic,[1,*] Ingo Grevemeyer,[2] Joerg Bialas[2] and C. Joerg Petersen[2]

[1] *Sonderforschungsbereicht* 574, *Wischhofstrasse* 1-3, 24148 *Kiel, Germany*
[2] *Leibniz Institut fuer Meereswissenschaften, IFM-GEOMAR, Wischhofstrasse* 1–3, 24148 *Kiel, Germany.*
E-mail: igrevemeyer@ifm-geomar.de

Accepted 2009 December 6. Received 2009 November 15; in original form 2008 December 17

SUMMARY

Recent seismic evidence suggested that most oceanic plate hydration is associated with trench-outer rise faulting prior to subduction. Hydration at trenches may have a significant impact on the subduction zone water cycle. Previous seismic experiments conducted to the northwest of Nicoya Peninsula, Northern Costa Rica, have shown that the subducting Cocos lithosphere is pervasively altered, which was interpreted to be due to both hydration (serpentinization) and fracturing of the crustal and upper-mantle rocks. New seismic wide-angle reflection and refraction data were collected along two profiles, running parallel to the Middle American trench axis offshore of central Nicaragua, revealing lateral changes of the seismic properties of the subducting lithosphere. Seismic structure along both profiles is characterized by low velocities both in the crust and upper mantle. Velocities in the uppermost mantle are found to be in the range 7.3–7.5 km s^{-1}; thus are 8–10 per cent lower than velocities typical for unaltered peridotites and hence confirm the assumption that serpentinization is a common process at the trench-outer rise area offshore of Nicaragua. In addition, a prominent velocity anomaly occurred within the crust beneath two seamounts. Here, velocity reduction may indicate increased porosity and perhaps permeability, supporting the idea that seamounts serve as sites for water percolation and circulation.

Key words: Hydrology; Mantle processes; Earthquake dynamics; Seismic tomography; Subduction zone processes.

GJI Seismology

INTRODUCTION

To better understand the subduction zone dynamics it is important to determine the amount of water that is being subducted within the incoming oceanic plate into the deep subduction zone. The dehydration of the subducting slab at depth affects a number of processes in a subduction zone system, including dehydration-embrittlement causing intermediate-depth earthquakes. Further, water released from a subducting slab into the mantle wedge plays an important role in partial melting, controlling volcanic arc magmatism. It has been suggested that most oceanic plate hydration occurs in trench-outer rise area through bending-related faulting prior to subduction (e.g. Peacock 2001, 2004). This hypothesis is supported by seismological studies, which suggest that faults cut >20 km into the lithosphere (Kanamori 1971; Christensen & Ruff 1988; Hasegawa *et al.* 1994; Lefeldt & Grevemeyer 2008), allowing water to infiltrate and serpentinize the uppermost mantle. Multichannel seismic reflection (MCS) images of the subducting oceanic lithosphere offshore of Nicaragua (Ranero *et al.* 2003) suggest that trench-outer rise faults created prior to subduction cut through the entire crust into the upper mantle and may cause serpentinization. Serpentine could be the main slab water carrier to the deep mantle as antigorite, the high-pressure variety of serpentine, can remain stable down to ∼200 km depth in cold subduction zones (e.g. Ulmer & Trommsdorff 1995). Seismic compressional wave velocity decreases during serpentinization: from ∼8.0–8.2 km s^{-1} in non-serpentinized peridotites to ∼4.5 km s^{-1} at 100 per cent transformation of peridotite to serpentinite (Carlson & Miller 2003). Thus, seismic velocities are a good indicator for studying the impact of hydration on the lithospheric structure at mantle depth.

Previous active seismic experiments offshore of Nicoya Peninsula, Northern Costa Rica, conducted during the research vessel 'Sonne' cruise SO173–1 have revealed systematic changes in the seismic structure of the subducting Cocos lithosphere at the trench, indicating that bending-related faulting and hydration occurring in the trench-outer rise is an evolutionary process (Ivandic *et al.* 2008). Low compressional velocities and anomalous low heat flow values at the outer rise and features that might indicate infiltration of seawater and potential hydration of the oceanic crust and upper mantle. Previously, evidence for mantle rock alteration using seismic velocities derived from seismic refraction and wide-angle data has only been found at abandoned spreading ridges (Osler & Louden 1995; Grevemeyer *et al.* 1997) and interpreted in terms of hydration and

*Now at: Institut IGH d.d., Janka Rakuse 1, Zagreb 10000, Croatia. E-mail: mivandic@igh.hr

hence serpentinization. However, all previous surveys off Central America studying the state of hydration of the oceanic lithosphere prior to subduction (Ranero *et al.* 2003; Grevemeyer *et al.* 2007; Ivandic *et al.* 2008) collected data in the vicinity of the suture zone between crust created at the Cocos-Nazca spreading centre and the East Pacific Rise (EPR; Barkhausen *et al.* 2001). This area is known to be characterized by unusual hydrothermal activity in the incoming plate (Fisher *et al.* 2003a; Hutnak *et al.* 2008) that may facilitate water percolation down to mantle depth.

The aim of the R/V 'Meteor' cruise M66 Leg 4a was to conduct trench parallel seismic profiles to reveal along trench changes of the seismic properties of the lithosphere approaching the trench and to confirm the interpretation of seismic and seismological data that serpentinization is a common process offshore of Nicaragua. The two seismic profiles, p01 and p02, were acquired offshore off central Nicaragua. Both profiles survey the trench where bending of the subducting plate is much stronger than offshore Nicoya peninsula, where previous seismic work has been conducted. If bending is indeed causing hydration of the mantle prior to subduction, we would expect a much larger velocity anomaly than observed further to the south (Grevemeyer *et al.* 2007; Ivandic *et al.* 2008). In this paper, we present the resulting velocity structures along the two seismic profiles, derived from joint refraction/reflection seismic tomography (Korenaga *et al.* 2000). The velocity models were used to infer the degree of hydration of the subducting lithosphere along the trench axis, as well as to examine the impact of seamounts on hydration processes in the lithospheric rocks and changes in their seismic properties. The uncertainties of the models are estimated by applying a Monte Carlo analysis. Resolution tests are also performed to evaluate the resolving power of the data set.

TECTONIC FRAMEWORK

The study area of the cruise M66–4a is located offshore of central Nicaragua seaward of the Middle American trench, where the Chocos plate subducts beneath the Carribbean plate with a rate of about 91 mm yr^{-1} (DeMets *et al.* 1990) in a northeasterly direction. The topography of the incoming plate reveals that seafloor spreading and magnetic anomalies off Nicaragua strike almost parallel to the trench axis (Barkhausen *et al.* 2001). The subducting ~24 Myr old Cocos lithosphere formed at the fast-spreading EPR is pervasively faulted with offsets of up to 500–700 m on back-tilted normal faults (Ranero *et al.* 2003). This is associated with extensional tectonics caused by the flexure of the subducting crust. MCS data suggest that the faults cut the lithosphere down to 18–20 km depth (Ranero *et al.* 2003). Further to the south, the fault offsets decrease to <200 m as the plate approaches Nicoya Peninsula. Swathmapping bathymetric data show that offshore of central Nicaragua the system of half-grabens is much broader and faults parallel to the trench are more prominent and wider than anywhere else in the region (Fig. 1; Ranero *et al.* 2003), indicating more pervasive faulting of the subducting lithosphere.

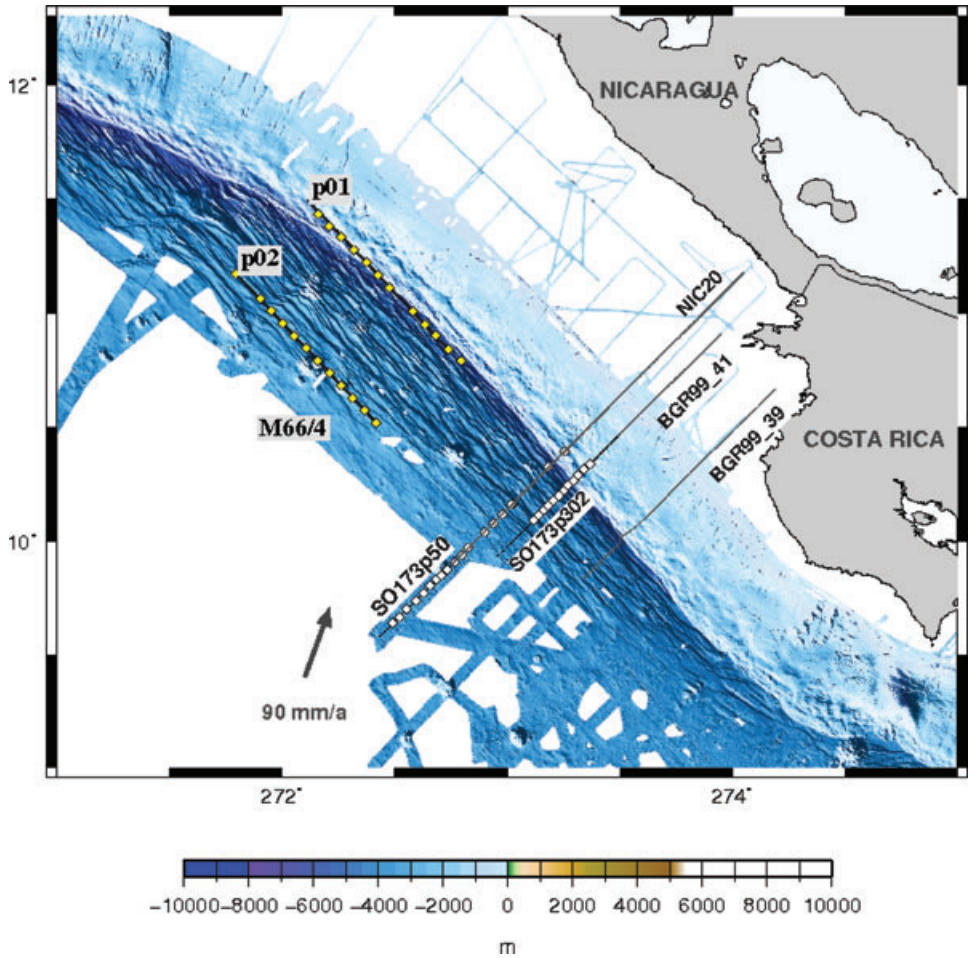

Figure 1. Bathymetry map of the offshore region of northwestern part of Nicaragua. Thick solid lines designated p01 and p02 are the seismic profiles conducted during the Meteor M66-4a cruise, with instrument locations denoted by squares. The profiles run parallel to the Middle America Trench.

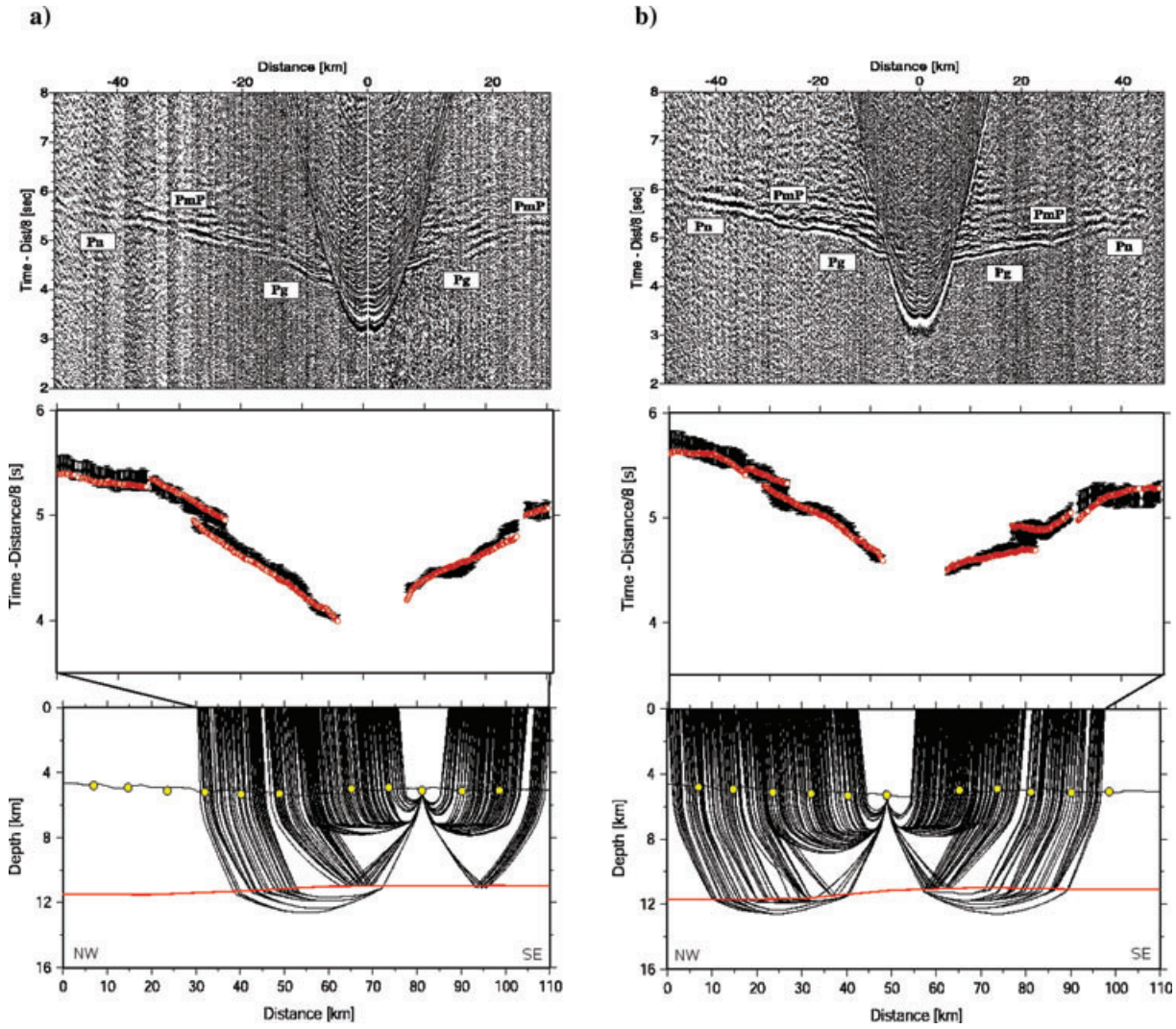

Figure 2. (a) Observed seismic record sections from selected instruments from the profile p01. Data have been reduced to 8 km s^{-1} and bandpass filtered between 5 and 30 Hz. Wide-angle data examples from the profile p01 are shown for OBS35 and OBS37. Picked traveltimes (solid circles with error bars) and predicted traveltimes (red circles) for *Pg*, *PmP* and *Pn* phases are shown in the middle plots. Corresponding ray paths are plotted at the bottom. OBS 35. (b) Continued. OBS 37.

An outer rise seismological monitoring network, deployed over a time period of 33 days in 2003 July and August offshore of Nicoya Peninsula, detected high seismicity rate with approximately three local microearthquakes per day, indicating that normal faults are continuously active (Grevemeyer *et al.* 2007). In 2005 October and November a second network was deployed off central Nicaragua, where bending is most profound in bathymetric data. Here, earthquakes with M_w of ∼1.2–2.9 occur down to ∼15 km below sea level, cutting 5–10 km into the mantle (Lefeldt *et al.* 2009). However, large earthquakes ($M_w > 6$) recorded at teleseismic distances may suggest that trench-outer rise normal faults cut down to even greater depth, yielding centroid depths of 10–25 km for events from Central America (Lefeldt & Grevemeyer 2008).

SEISMIC EXPERIMENT AND DATA

The two wide-angle and refraction profiles, p01 and p02, were conducted in 2005 November during the research vessel Meteor 66–4a cruise (Fig. 1). They were conducted seaward of the trench in the outer rise area offshore of central Nicaragua. The instruments were deployed at intervals of ∼5 nm.

As a seismic source we used an array of four G-gun clusters with a total volume of 64 l of air compressed at 210 bars and were towed at a water depth of 5 m. The array was fired at intervals of 60 s, resulting at ship's speed of 4.5 kn into an average spacing of 130 m. Figs 2 and 3 show examples of the data quality available for data inversion. 12 ocean bottom seismographs (OBS; Bialas & Flueh 1999) and ocean bottom hydrophones (OBH; Flueh & Bialas 1996) were deployed along each line.

Profile p01 is 120 km long and runs along the trench axis and intersects the trench at 11°N, ending in the margin wedge at its northwestern part. Unfortunately, one station deployed on the top of the margin wedge did not provide data for geophysical interpretation.

The 120-km-long profile p02, with the same orientation as the profile p01, is located ∼60 km seaward of the trench axis. Data from both lines passed an anti-aliasing filter of 50 Hz and were continuously recorded with a sampling rate of 200 Hz on all OBH and OBS stations. The data were played back and split into single shot

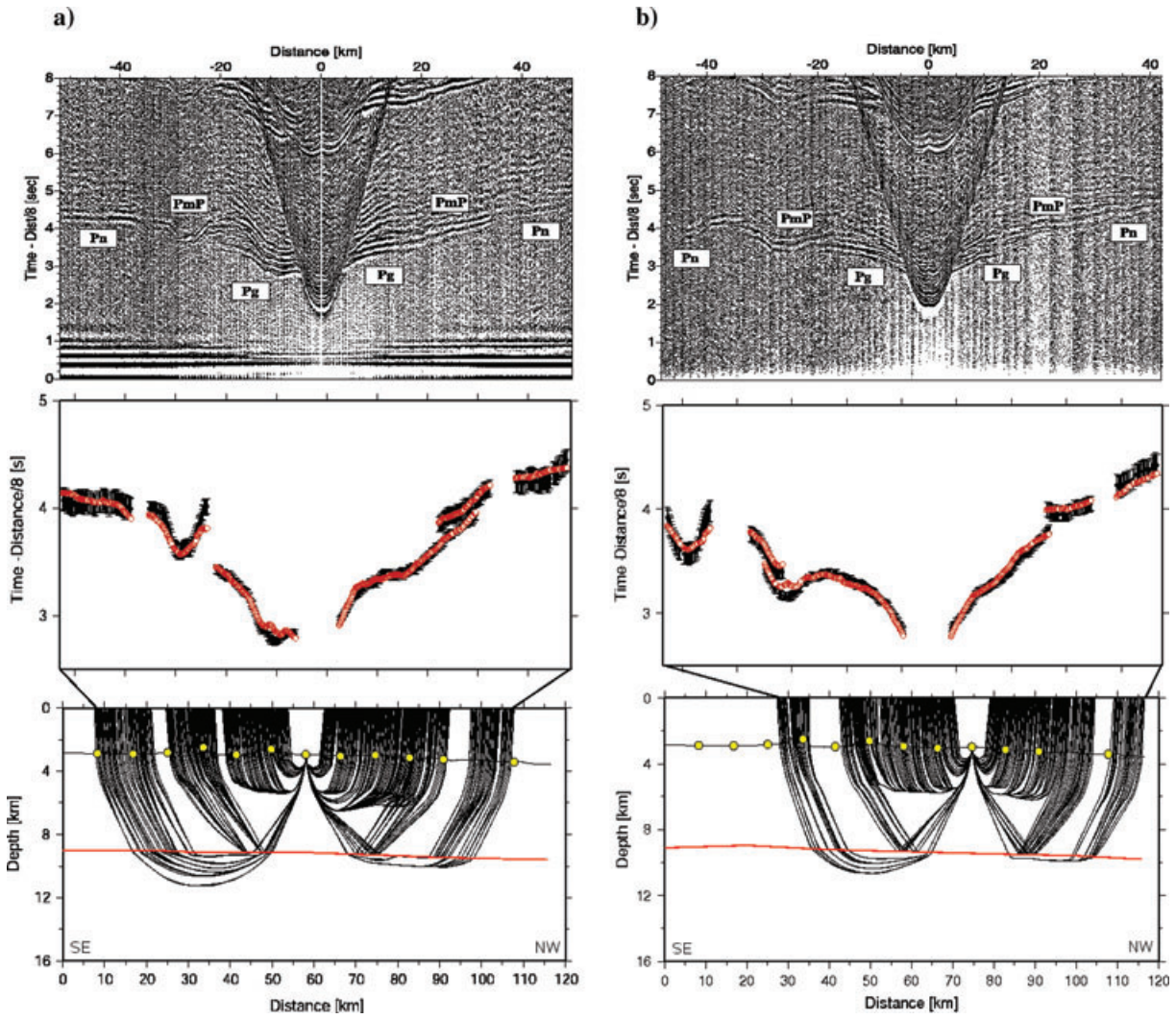

Figure 3. (a) Same as in the Figs 2 and 3 for profile p02. OBH 27. (b) Continued. OBH 43.

records stored as a receiver gather in SEG-Y format. The instruments were deployed by free fall, using Global Positioning System (GPS) for drop-point positioning; instrument locations were further constrained using water-path traveltimes from the shots collected while the ship was navigated with GPS. Spectral analysis and filter tests show that the seismic energy is in a band ranging from 4 to 25 Hz. We ran this test for both near-offset and far-offset traces and chose a time- and range-dependant bandpass filtering approach. In addition, amplitudes were multiplied by distance to partly compensate the spherical divergence, simultaneously showing the level of both seismic signal and ambient noise phase quality.

The seismic structure of the subducting oceanic lithosphere is constrained by crustal refractions (*Pg*), Moho reflections (*PmP*) and upper-mantle refractions (*Pn*). Average picking uncertainties are ∼30–40 ms at near offsets and ∼90 ms at far offsets for refracted arrivals, and ∼70 ms for *PmP* phases.

Crust subducting at the Middle America trench has been created roughly 24 Myr ago at the EPR (Barkhausen *et al.* 2001). Oceanic crust generated at mid-ocean ridges is fundamentally different from continental crust (e.g. Raitt 1963) and a wealth of seismic refraction studies collected over more than 40 yr in the ocean basins suggest that the upper crust (layer 2) is a region of strong velocity gradient (∼1 km s^{-1} km^{-1}), whereas the lower crust (layer 3) is relatively homogeneous, although it does show an increase in velocity with depth (0.1–0.2 km s^{-1} km^{-1}; e.g. Kennett & Orcutt 1976; Whitmarsh 1978). The thickness of the layer 2 is typically ∼1.5 km and the velocities for mature range from 3.8–4.8 km s^{-1} at the top to 6.2–6.7 km s^{-1} at the bottom. The velocities of the layer 3 increase from 6.7–6.8 km s^{-1} at the top of the layer to 7.0–7.2 km s^{-1} at the Moho boundary (e.g. White *et al.* 1992; Grevemeyer *et al.* 1998). More recent studies have subdivided the upper crust in layer 2a, composed of extruded basalts, and layer 2b, formed by basaltic sheeted dikes (e.g. Christeson *et al.* 1996). Oceanic crust, however, show some variability (e.g. White *et al.* 1992). We therefore used a wide range of different starting models reflecting the variability inherently associated with crustal accreting at spreading ridges. Our starting models (see Monte Carlo analysis) cover roughly the range of mature oceanic crust given by White *et al.* (1992). Crustal thickness has been between 5 and 6.5 km, reflecting the variability in the East Pacific (e.g. Grevemeyer *et al.* 1998). Velocity of the uppermost mantle just below the Moho was 8.0 km s^{-1}, typical of olivine-rich peridotites. The overall structure of the reference crust (Fig. 8), however, resembles Pacific crust sampled elsewhere (e.g. White *et al.* 1992).

The main aim of this study is to reveal lateral changes in the seismic structure of the subducting oceanic crust and upper mantle

that might be associated with bending-related faulting and hydration occurring in the outer rise-trench region. In the end, the results would reveal if serpentinization is a common process at the deep-sea trench offshore of Nicaragua.

TOMOGRAPHIC INVERSION

The velocity–depth model was obtained using a joint refraction and reflection traveltime inversion approach of Korenaga *et al.* (2000) that simultaneously solves for the seismic velocity field and the depth of a reflecting interface (i.e. seismic Moho). The geometry of the Moho is constrained as a floating reflector with nodes with just one degree of freedom in the vertical direction. The traveltimes and ray paths are calculated using a hybrid ray tracing scheme based on the graph method (Moser 1991) and the ray-bending refinement (Moser *et al.* 1992). We performed inversion in layer stripping fashion; first the oceanic crust was constrained by inverting the *Pg* phases simultaneously with the *PmP*, and then the *Pn* phases were included together with the structural information above the Moho interface gained from *Pg* and *PmP* inversion.

The data set of the profile p01 consisted of 2658 *Pg,* 1126 *PmP* and 834 *Pn* phases that were handpicked from 11 instruments. The model is 110 km long and 20 km deep and is parametrized as a sheared mesh hanging from the seafloor topography with 0.5 km lateral nodal spacing, whereas vertical node spacing ranges from 0.05 km at the top to 0.5 km at the bottom of the model. The Moho depth nodes spaced every 1 km define the floating reflector. The inversion is stabilized by adding smoothness correlation lengths, one each in the horizontal and vertical directions for the velocity nodes and one for the depth nodes. The horizontal correlation length values vary from 3 km at the top of the model to 8 km at the bottom, and vertical correlation lengths increase from 0.1 km at the top to 3 km at the bottom. The depth sensitivity is weighted by a depth kernel weighting parameter w. For the inversion of *Pg* and *PmP* phases we used $w = 1$, which means that velocity and depth nodes are equally weighted. For the final inversion step, where all the phases were included, this parameter had a value of 0.1, allowing more perturbations for the velocity than for the depth. Inversion of traveltime residuals was completed in five iterations, giving a final rms misfit of 56 ms ($\chi^2 = 1.16$). Picked and calculated traveltimes, and ray tracing examples of two ocean bottom instruments are shown in Figs 2(a) and (b).

In the inversion of the data set of the profile p02 we used similar parametrization. The horizontal grid spacing is 0.5 km, and vertical grid nodes are 0.05 km distant at the top of the model and about 0.6 km at the bottom. The Moho depth nodes are 1 km spaced. The horizontal correlation lengths range from 3 km at the top to 7 km at the bottom, and the vertical correlation lengths are the same like in the profile p01. All the crustal and upper-mantle phases recorded along both profiles are of a good quality on almost all stations. In total 2855 *Pg*, 1124 *PmP* and 1189 *Pn* were handpicked from 12 stations and inverted. Five iterations were enough to obtain a good fitting between the observed and calculated traveltimes with the final rms of 57 ms ($\chi^2 = 1.08$). Picked and calculated traveltimes, and ray tracings from two ocean bottom instruments from that profile are shown in Figs 3(a) and (b).

RESOLUTION AND MODEL UNCERTAINTY

The sensitivity of our final model to different input models was estimated by averaging the solutions of 100 Monte Carlo realizations (e.g. Korenaga *et al.* 2000). Starting models roughly cover the range of seismic velocities found in mature Pacific crust (White *et al.* 1992). The degree of dependence of the final solution on the starting model can be assessed by conducting a number of inversions with a variety of randomly generated initial models and noisy data sets. If all models have the same probability and the starting models cover the full region of non-null probability within the parameter space, the *a posteriori* covariance of the solutions can be interpreted as a statistical measure of the model uncertainties (Tarantola 1987). To estimate the velocity and Moho depth uncertainty we apply a similar approach as the one described in Sallares *et al.* (2003). A set of 1-D reference models was constructed for both profiles by randomly varying the Moho depth ($\sigma = 0.5$ km) and the velocity ($\sigma = 0.3\,\mathrm{km\,s^{-1}}$) and inverting them with noisy data sets constructed by adding random picking errors ($\pm$20 ms), together with the common phase errors ($\pm$50 ms) and common receiver errors ($\pm$50 ms) to the initial data set.

The velocity uncertainty is lower than $0.1\,\mathrm{km\,s^{-1}}$ within most parts of the models, both in the crust and upper mantle, indicating that velocity anomalies are well recovered (Figs 4a and b). Moho depth uncertainty along the major part of the profile p01 is not higher than 0.15 km. Maximum values of 0.2–0.25 km are found in the part which extends into the lower continental slope area. Uncertainty of the Moho depth along the entire profile p02 is as low as 0.15 km, except for the northwestern edge, where it reaches 0.3 km. The estimated uncertainties indicate that the model parameters are well constrained along both profiles, confirming the robustness of our iterative scheme.

The derivative weight sum (DWS) describes the relative ray density near a given velocity node, providing crude information on the model resolution (Toomey & Foulger 1989). The DWS values show good ray coverage, hence generally good resolution for both velocity models (Figs 6b and 7c), coinciding with the small uncertainties estimated by Monte Carlo approach.

However, to quantitatively assess resolution and explore whether our data set can resolve anomalous crustal velocity zone beneath the seamounts, we created synthetic models using the final velocity model with and without $\pm$6 per cent Gaussian anomalies placed in between 5 and 9 km depth. Synthetic data sets have been calculated for the synthetic velocity model with the same source-receiver geometry as in the real data set. Random noise with rms amplitude of the picking errors has been added to the synthetic traveltimes obtained from the perturbed velocity model. The results of the inversion reveal that the velocity anomaly is well recovered, showing only small difference of $\sim$1 per cent between the synthetic and recovered anomaly (Fig. 5). Thus, the resolving power of our data set is good enough to fully resolve features similar to the anomaly found beneath the seamounts.

RESULTS

The seismic structure along both profiles is quite similar. The crust in this region is about 5.6–5.8 km thick. The sediment thickness of $\sim$400–500 m is quite uniform along the lines, except in the $\sim$30 km of the northwestern part of the profile p01, which extends into the lower continental slope, and where it is larger by up to $\sim$500 m. The velocity of the sediment cover ranges from $1.65–1.9\,\mathrm{km\,s^{-1}}$. The 2-D *P*-wave velocity model of the profile p01 with the reflector geometry obtained after five iterations is shown in the Fig. 6(a).

The crustal and upper-mantle velocities are strongly reduced compared to velocities expected for $\sim$24 Myr old mature

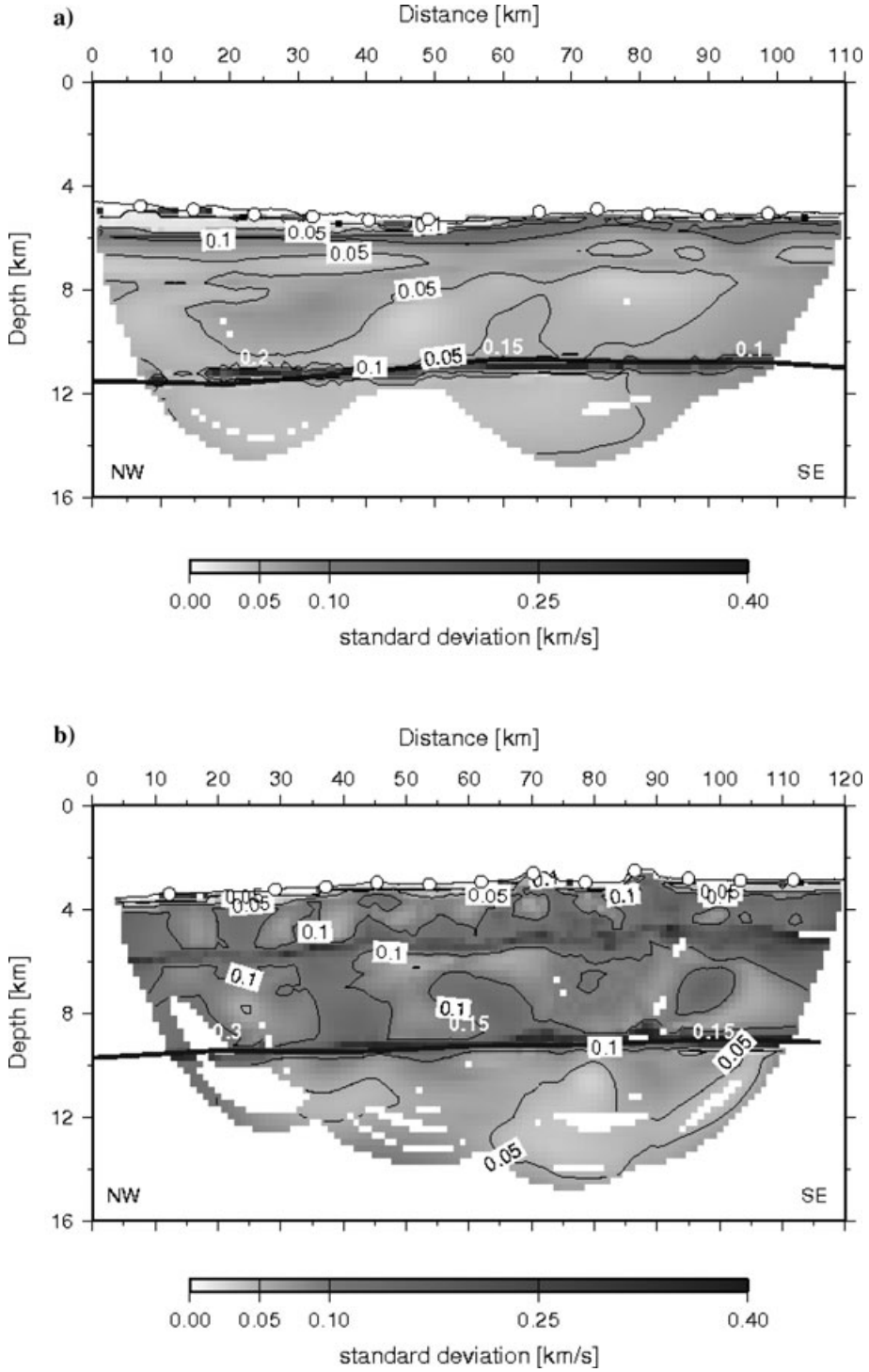

Figure 4. Velocity and Moho depth uncertainties estimated from the Monte Carlo analysis for (a) profile p01 and (b) profile p02. The estimated velocity uncertainties, which are not higher than 0.05–0.1 km s^{-1} both in the crust and upper mantle, indicate that the models are well constrained.

oceanic lithosphere (Grevemeyer & Weigel 1996; Carlson 1998; Grevemeyer & Bartetzko 2004) and velocities found seaward of the trench-outer rise (Wilson *et al.* 2003; Ivandic *et al.* 2008), indicating alteration in seismic and chemical properties of the rocks. Velocities in layer 2 increase from ∼3.8–4.0 km s^{-1} at its top to ∼5.9–6.1 km s^{-1} at the boundary with the layer 3. With respect to crust sampled seaward of the trench-outer rise (Wilson *et al.* 2003; Ivandic *et al.* 2008), reduced velocities are also typical for the layer 3 and range from ∼6.2–6.3 km s^{-1} at the top to 6.5–6.6 km s^{-1} at the bottom just above the Moho interface (Fig. 8). Below the Moho the upper-mantle rocks with velocities of 7.2–7.5 km s^{-1} are found along the entire profile.

The final velocity model of the profile p02 is shown in Fig. 7(a). Velocities of the layer 2 range from ∼4.0–4.2 km s^{-1} at the top of the layer to ∼6.0–6.2 km s^{-1} at the bottom. The velocities at the top of the layer 3 are ∼6.3 – 6.4 km s^{-1} and increase to ∼6.6 km s^{-1} at the

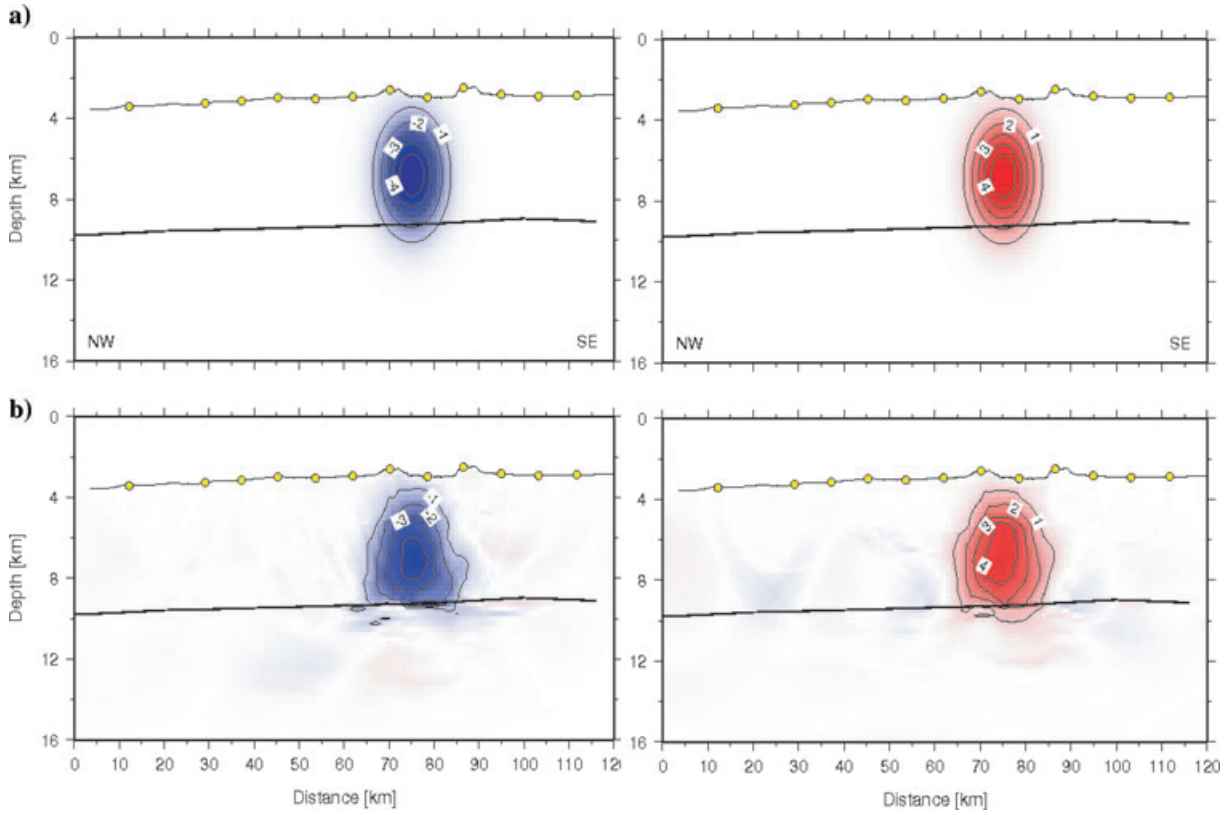

Figure 5. Results of the resolution tests for the profile p02; crustal anomalies beneath the seamounts along the profile p02. (a) Velocity anomalies of ±6 per cent in the synthetic models are given with respect to the final model displayed in Fig. 6(a). (b) Recovered anomalies.

Moho boundary. Below Moho, upper mantle velocities are strongly reduced and have similar values as those found at the profile p01, that is, they are not higher than 7.3–7.5 km s^{-1}. One explanation for this unexpected observation is that the emplacement of the seamounts has inherently affected both crustal and upper mantle velocities, masking any evolutionary effect caused by bending-related faulting.

Another interesting feature is related to the two seamounts, which intersect the profile p02 in its southeastern part. Here, we observed crustal seismic velocities roughly 0.2 km s^{-1} lower than anywhere else along the profile. This profound velocity anomaly can best be traced by following the isolines. Along p02 the isovelocity contour of 6.5 km s^{-1} defines an area were the steep upper crustal gradient turns into a low gradient layer, interpreted to be the layer 2/layer 3 boundary. Along most of the profile the isovelocity contour runs horizontally. Under the seamounts, however, velocities are significantly reduced. Here the 6.5 km s^{-1} contour reaches even Moho depth.

Alterations in the seismic structures are uniformly present along both profiles. Fig. 8 shows seismic velocity–depth profiles at two selected locations along the profile p01 in comparison with the velocity structure seaward of the outer rise before bending related faulting affected the subducting plate (Wilson *et al.* 2003; Ivandic *et al.* 2008), suggesting that seismic velocity is profoundly lower in the trench.

DISCUSSION

The observed reduced seismic velocities in the crust and upper mantle along the two profiles running parallel to the trench axis indicate alterations of chemical and physical properties of the subducting lithospheric rocks offshore of northern Nicaragua. Multibeam bathymetry data reveal prominent faults, which extend far seaward of the trench, indicating that the plate is affected by large bending stresses, perhaps causing large-scale normal faulting and widespread hydration (serpentinization) of the crustal and upper-mantle rocks (Ranero *et al.* 2003). *P*-wave velocity models of the crust and upper mantle along the two profiles indeed support this hypothesis. Compared to velocities expected for ∼24 Myr old mature oceanic lithosphere (e.g. White *et al.* 1992; Carlson 1998; Grevemeyer & Bartetzko 2004), crustal velocities are reduced by 15–20 per cent at the top of the basaltic layer and by up to 8 per cent at the bottom. The lower gabbroic layer is characterized by ∼5 per cent velocity reduction. Upper-mantle velocities of 7.3–7.5 km s^{-1} are reduced by 8–10 per cent lower than those expected for unaltered peridotites. These velocity anomalies are uniform along the trench axis and stronger than those found in the profile perpendicular to the trench further south (Grevemeyer *et al.* 2007; Ivandic *et al.* 2008). The magnitude of the uppermost mantle velocity anomaly corresponds to the amount of faulting that can be assessed using swathmapping bathymetry. Thus, seafloor is much rougher off central Nicaragua, which is related to stronger bending of the subducting plate, causing large-scale faulting of the brittle lithosphere (e.g. Ranero *et al.* 2003; Lefeldt & Grevemeyer 2008). Pervasive fracturing facilitates seawater percolation and hydrothermal flow through the incoming plate. This is supported by a significant decrease in heat flow approaching the trench axis, indicating that bending-related faulting may govern hydrothermal circulation within the crust prior to subduction (Grevemeyer *et al.* 2005). The fact that bending-related is more profound in seafloor bathymetry may

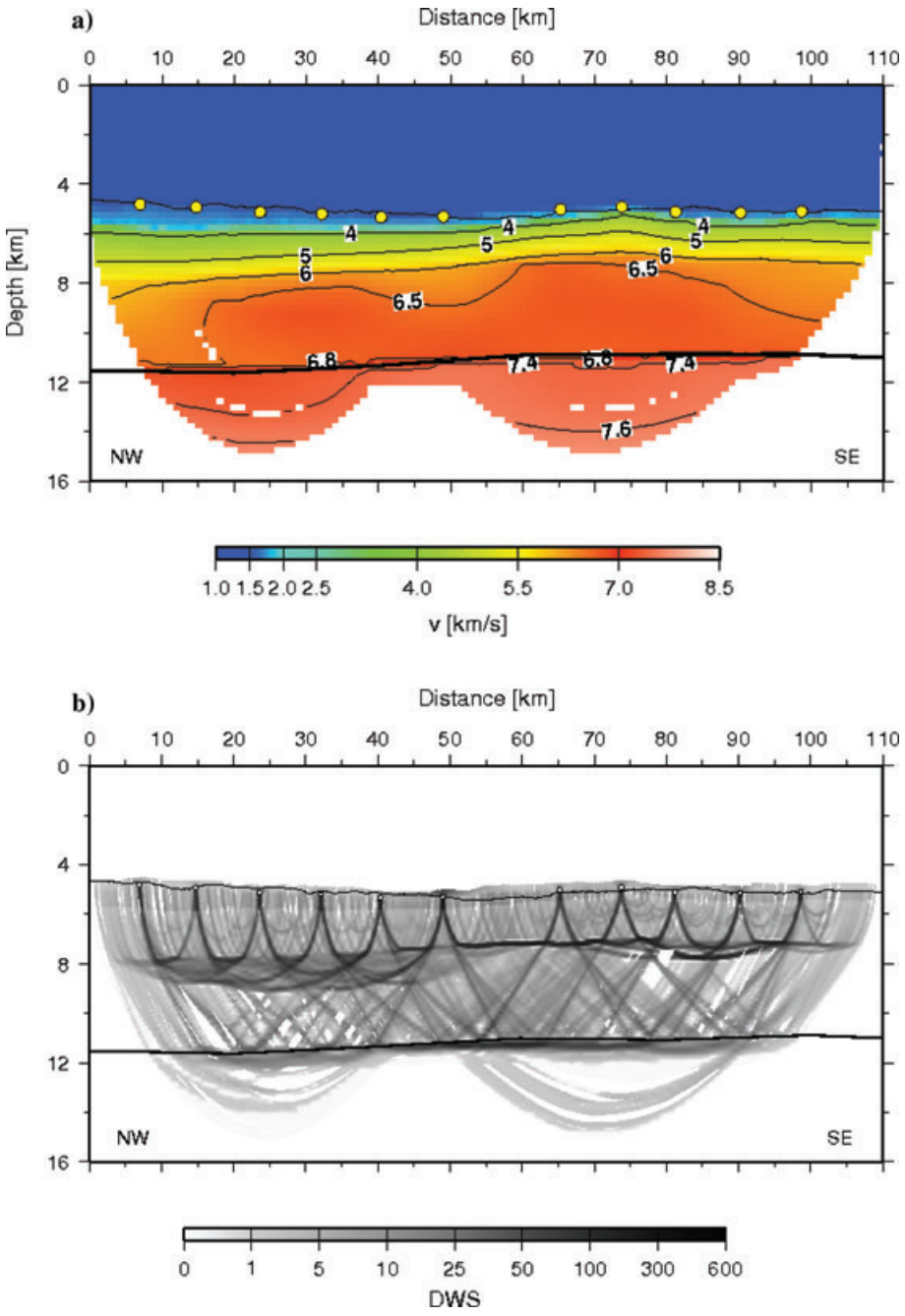

Figure 6. (a) *P*-wave velocity model for the profile p01. (b) Derivative weight sum.

support the interpretation that water percolation is more vigorous and hence serpentinization is far more advanced than offshore Nicoya peninsula (Ivandic *et al.* 2008), resulting in lower-mantle velocities.

A certain degree of the azimuthal seismic anisotropy could also arise from the lattice-preferred orientation (LPO) of the minerals. Tectonic plate motion is thought to cause solid-state plastic flow within the underlying upper mantle and accordingly lead to the development of a LPO of the constituent olivine crystals, which stabilizes during spreading and attenuates during subduction. The mechanical anisotropy that results from such a preferred orientation typically produces a direction of maximum seismic wave velocity parallel to the plate motion direction. Azimuthally varying *Pn*-wave velocities were first recorded in the shallow upper mantle beneath Hawaii (Hess 1964), showing that surface waves travel ∼10 per cent faster in spreading direction than in the ridge crest parallel direction. The degree of compressional wave anisotropy depends also on spreading rates, so while 3–4 per cent have been found in the slow-spreading North Atlantic (Keen & Tramonti 1970; Gaherty *et al.* 2004), >7 per cent has been observed near the fast-spreading EPR (Dunn *et al.* 2000). Much lower degree of *Pn* anisotropy has been found offshore of Southern Central Chile, in the trench-outer rise area of the oceanic Nazca plate created at the fast-spreading Chile Rise. Comparison of the uppermost mantle velocities at the crossing points of perpendicular profiles revealed <2 per cent degree of *Pn* anisotropy (Contreras-Reyes *et al.* 2008a). A lower degree of anisotropy that has been found in the outer-rise environment or in ophiolites (e.g. Schmitt *et al.* 2007) has been proposed to reflect

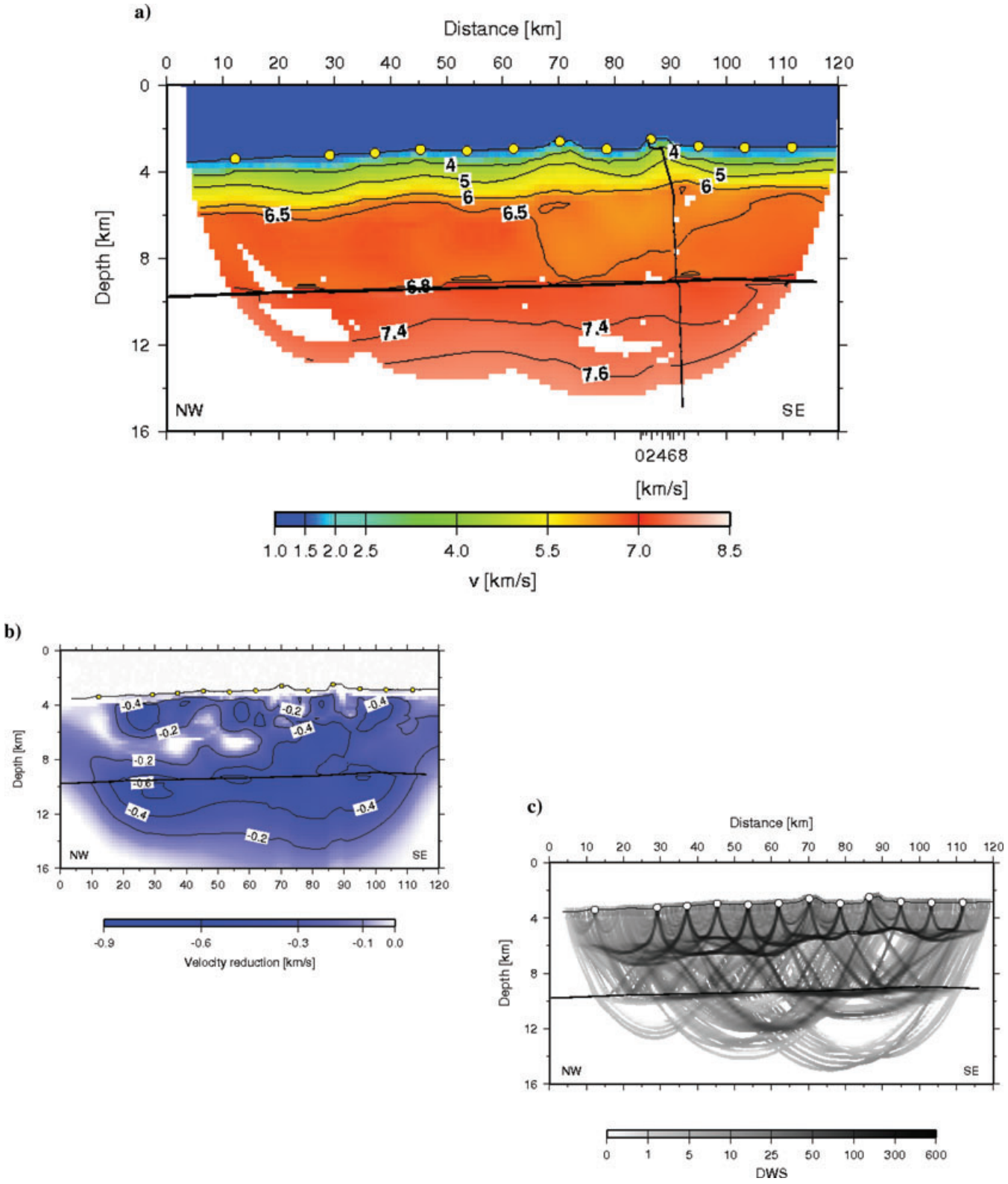

Figure 7. (a) *P*-wave velocity model for the profile p02 with the 1-D velocity profile at the seamount. The distance scale coincides with the distance scale in the refraction profile. (b) Velocity reduction with respect to an unaltered oceanic lithosphere found seaward of the trench-outer rise area (Wilson *et al.* 2003; Ivandic *et al.* 2008). (c) Derivative weight sum.

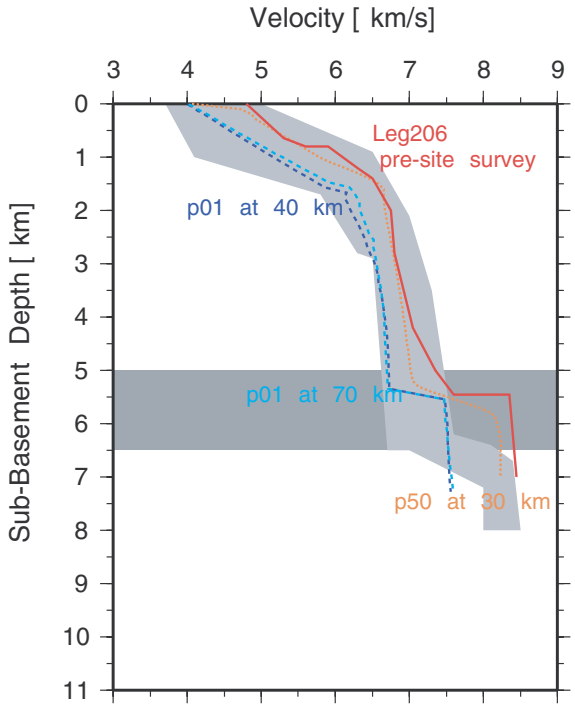

Figure 8. Velocity–depth profiles at two selected locations along the profile p01, and comparison with the velocity structure seaward of the outer rise before bending-related faulting affected the subducting plate (Wilson *et al.* 2003, P50, Leg 206; Ivandic *et al.* 2008), suggesting that seismic velocity is profoundly lower in the trench. Light grey shaded area provides the variability of seismic velocity for mature Pacific crust (White *et al.* 1992) and dark grey shaded area the thickness variability. For the Monte Carlo inversion, grey areas cover the boundaries of 100 random starting models.

an increased degree of serpentinization, because of the random orientation of serpentine minerals, which replace preferentially aligned olivines.

Another distinctive feature in the model of the p02 profile is a significant velocity reduction in the crustal layer beneath two seamounts. Velocities are reduced by $\sim$0.2 km s^{-1} compared to the surrounding crust, indicating increased porosities associated with seamounts, either related genetically to seamount emplacement (i.e. compositional changes) or related to focused faulting and hence fracture porosity under seamounts.

The anomalous behaviour in the upper and lower crust is confined to the seamount area and extends down to the Moho boundary. This result is in agreement with the hypothesis that seamounts facilitate inflow of seawater into the oceanic crust and might guide hydrothermal circulation between sites separated by large distances (Fisher *et al.* 2003b). Fisher *et al.* (2003b) have found that seawater can flow over lateral distances of at least $\sim$50 km through the crustal rocks before it discharges through an another seamount. In addition, recent numerical models of coupled heat and fluid transfer suggest that seamounts play an important role in the exchange of fluid and heat between the crust and ocean (Harris *et al.* 2004). However, another interpretation of the velocity anomaly under the seamounts might be related to the composition of crust. Thus, local heterogeneous composition of the mantle source could account for lower crustal velocities and enhanced volcanism (Korenaga *et al.* 2002). In this model the emplacement process rather than porosity structure is governing the lateral variability of seismic velocity under the seamounts.

Conductive lithospheric cooling models predict a heat flux of $\sim$100 mW m^{-2} for $\sim$18–24 Ma oceanic crust (Stein & Stein 1994). Heat flux data, however, show that heat flux through the seafloor created at the EPR is anomalously low, with values in between 20 and 40 mW m^{-2} (Langseth & Silver 1996; Fisher *et al.* 2003a; Grevemeyer *et al.* 2005; Hutnak *et al.* 2008), which is only $\sim$30 per cent of the values predicted by these models. This anomalously low heat flux is attributed to effective hydrothermal cooling of the upper oceanic crust, which is facilitated by seamounts and basaltic outcrops (Silver *et al.* 2000; Hutnak *et al.* 2008). In addition, Grevemeyer *et al.* (2005) show that heat flow decreases towards the trench axis, whereas the number of faults and fault offset increases, suggesting that faulting governs hydrothermal activity in the trench-outer rise.

Low upper mantle velocities observed seaward of deep sea trenches have been interpreted to be caused by serpentinization of the dry peridotites (Contreras-Reyes *et al.* 2007, 2008b; Grevemeyer *et al.* 2007; Ivandic *et al.* 2008). We estimate that in this area the uppermost $\sim$4 km of the mantle might contain up to $\sim$19–24 per cent of serpentine, corresponding to a water content of $\sim$2.5–3.1 weight per cent (Carlson & Miller 2003). The serpentinized peridotite hypothesis is supported by the frequency–magnitude distribution of local earthquakes recorded in the area of our seismic deployment (Lefeldt *et al.* 2009). The *b*-value significantly increases from $b = 1.2$ away from the trench axis to $b = 2.3$ within 20 km of the trench. Thus, in the vicinity of the trench the lithosphere ruptures more frequently, but under the release of less energy, implying that the rheology of the lithosphere has weakened drastically and that only relatively deep earthquakes with a compressional fault mechanism show comparable large moment magnitudes (Lefeldt *et al.* 2009). The observed rheological weakening may indicate the presence of serpentine, which, even in small amounts, profoundly reduces the strength of an altered peridotite (Escartin *et al.* 2001).

Highly serpentinized mantle within the subducting Cocos slab offshore of Nicaragua would be also consistent with the fact that the Nicaraguan volcanic arc shows globally the highest concentrations of geochemical tracers for oceanic crustal fluid (e.g. boron). Ratios such as B/La, Ba/La and Be/Be indicate that subducted slab signal is the greatest in the Nicaraguan arc, where the dip is the steepest, and decreases towards Costa Rica to its minimum (Carr *et al.* 1990; Morris *et al.* 1990; Leeman *et al.* 1994). One interpretation is that Be and B are efficiently removed from the slab by the slab-derived fluids (Turner *et al.* 1998). However, the location of the water reservoir is still under debate, as it could reside either in the subducted oceanic lithosphere or in the mantle wedge. Tonarini *et al.* (2007) suggest a model in which tectonic erosion, that is, dragging down of slivers of serpentinized upper plate mantle, is responsible for the occurrence of serpentinite reservoir, 11B-enriched in the forearc by shallow fluids. Ruepke *et al.* (2002), however, proposed that the stronger slab signal in Nicaraguan, compared to Costa Rican arc lavas, reflects greater amounts of fluid released from the dehydration of more extensively serpentinized slab mantle.

Seismological constraints from the downgoing plate at a depth of 70–150 km under Nicaragua support the idea that serpentinization has indeed affected the subducting lithosphere (Syracuse *et al.* 2008). It is interesting to note, however, that the thermal structure of the subducting plate (Peacock *et al.* 2005) may not promote shallow dehydration (i.e. under the arc) of serpentinites trapped in the mantle, but at greater depth (>150–200 km). Thus,

water trapped in the mantle is transported into the deep Earth's interior.

CONCLUSIONS

A previous seismic experiment, acquired in the outer rise-trench region offshore of southern Nicaragua (Ivandic *et al.* 2008) revealed that bending-related faulting in the trench-outer rise is an evolutionary process in the subducting Cocos lithosphere. To investigate if serpentinization is a characteristic feature for the entire subducting lithosphere offshore of Nicaragua, we surveyed two trench parallel profiles offshore of central Nicaragua, profile p01 was located in the trench axis, and profile p02 runs ∼60 km seaward of profile p01. With respect to normal oceanic crust away from the area affected by trench-outer rise processes, seismic velocities of the crust and upper mantle are found to be significantly reduced along both profiles; velocities of the crust are reduced by 0.4–0.7 km s^{-1} and upper-mantle velocities are not higher than 7.3–7.5 km s^{-1}. These results confirm the assumption that serpentinization of the upper mantle is a common feature in the subducting lithosphere and that the uppermost 3–4 km of the mantle might be highly serpentinized, by up to 24 per cent. Other mechanisms, except hydration (serpentinization), that could contribute to the altered seismic properties, and thus should be considered when interpreting the results, are normal faults and fractures related to bending-related faulting and preferred orientation of the minerals.

Another interesting feature is a very prominent velocity anomaly in the crust below two seamounts. Crustal velocity here is reduced by 0.2 km s^{-1} compared to the other parts of the profile, suggesting increased porosity which may enhance water inflow into the upper and lower crust, and perhaps facilitate water migration down to mantle depth.

ACKNOWLEDGMENTS

We are grateful to the master, officers and crew of R/V Meteor cruise M66/4a for their excellent support at sea and to Klaus–Peter Steffen for operating and handling the airguns. We appreciate comments from two referees. This study was funded by the German Science foundation (DFG) through the SFB 574 'Volatiles and fluids in subduction zones' at Christan-Albrechts University, Kiel. SFB 574 contribution no. 177.

REFERENCES

Barkhausen, U., Ranero, C.R., von Huene, R., Cande, S.C. & Roeser, H.A., 2001. Revised tectonic boundaries in the Cocos plate off Costa Rica: implications for the segmentation of the convergent margin and for plate tectonic models, *J. geophys. Res.,* **106,** 19 207–19 220.

Bialas, J. & Flueh, E.R., 1999. Ocean bottom seismometers, *Sea Technol.*, **40**(4), 41–46.

Carlson, R.L., 1998. Seismic velocities in the uppermost oceanic crust: age dependence and the fate of layer 2A, *J. geophys. Res.,* **103,** 7069–7077.

Carlson, R.L. & Miller, D.J., 2003. Mantle wedge water contents estimated from seismic velocities in partially serpentinized peridotites, *Geophys. Res. Lett.,* **30**(5), doi:10.1029/2002GL016600.

Carr, M.J., Feigenson, M.D. & Bennet, E.A., 1990. Incompatible element and isotopic evidence for tectonic control of source mixing and melt extraction along the Central America arc, *Contrib. Mineral. Petrol.,* **105,** 369–380.

Christensen, D.H. & Ruff, L.J., 1988. Seismic coupling and outer rise earthquakes, *J. geophys. Res.,* **93**(B11), 13 421–13 444.

Christeson, G.L., Kent, G.M., Purdy, G.M. & Detrick, R.S., 1996. Extrusive thickness variability at the East Pacific Rise 9°–10°N: constraints from seismic techniques, *J. geophys. Res.,* **101,** 2859–2873.

Contreras-Reyes, E., Grevemeyer, I., Flueh, E.R., Scherwath, M. & Heesemann, M., 2007. Alteration of the subducting oceanic lithosphere at the southerncentral Chile trench–outer rise, *Geochem. Geophys. Geosyst.,* **8,** Q07003, doi:10.1029/2007GC001632.

Contreras-Reyes, E., Grevemeyer, I., Flueh, E.R., Scherwath, M. & Bialas, J., 2008a. Effect of trench-outer rise bending-related faulting on seismic Poisson's ratio and mantle anisotropy: a case study offshore of Southern Central Chile, *Geophy. J. Int.,* **173,** 142–156, doi:10.1111/j.1365-246X.2008.03716.x

Contreras-Reyes, E., Grevemeyer, I., Flueh, E.R. & Reichert, C., 2008b. Upper lithospheric structure of the subduction zone offshore of southern Arauco peninsula, Chile, at 38°S, *J. geophys. Res.,* **113,** B07303, doi:10.1029/2007JB005569, 2008

DeMets, C., Gordon, R.G., Argus, D.F. & Stein, S., 1990. Current plate motions, *Geophys. J. Int.,* **101,** 425–478.

Dunn, R.A., Toomey, D.R. & Solomon, S.C., 2000. Three-dimensional seismic structure and physical properties of the crust and shallow mantle beneath the East Pacific Rise at 9°30'N, *J. geophys. Res.,* **105,** 23 537–23 555.

Escartin, J., Hirth, G. & Evans, B., 2001. Strength of slightly serpentinized peridotites: implications for the tectonics of oceanic lithosphere, *Geology,* **29,** 1023–1026.

Fisher, A.T. *et al.,* 2003a. Abrupt thermal transition reveals hydrothermal boundary and role of seamounts within the Cocos Plate, *Geophys. Res. Lett.,* **30**(11), 1550, doi:10.1029/2002GL016766.

Fisher, A.T. *et al.,* 2003b. Hydrothermal recharge and discharge across 50 km guided by seamounts on a young ridge flank, *Nature,* **421,** 618–621.

Flueh, E.R. & Bialas, J., 1996. A digital, high data capacity ocean bottom recorder for seismic investigations, *Int. Underwater Syst. Des.,* **18**(3), 18–20.

Gaherty, J.B., Lizarralde, D., Collins, J.A., Hirth, G. & Kim, S., 2004. Mantle deformation during slow seafloor spreading constrained by observations of seismic anisotropy in the western Atlantic, *Earth planet. Sci. Lett.,* **228,** 255–265.

Grevemeyer, I. & Weigel, W., 1996. Seismic velocities of the uppermost igneous crust versus age, *Geophys. J. Int.,* **124,** 631–635.

Grevemeyer, I. & Bartetzko, A., 2004. Hydrothermal ageing of oceanic crust: inferences from seismic refraction and bore hole studies, in *Hydrogeology of Oceanic Lithosphere,* pp. 128–150, eds Davis, E.E. & Elderfield, H., Cambridge University Press, New York.

Grevemeyer, I., Weigel, W., Whitmarsh, R.B., Avedik, F. & Dehghani, G.A., 1997. The Aegir rift: crustal structure of an extinct spreading axis, *Mar. Geophys. Res.,* **19,** 1–23.

Grevemeyer, I., Weigel, W. & Jennrich, C., 1998. Structure and ageing of oceanic crust at 14°S on the East Pacific Rise, *Geophys. J. Int.,* **135,** 573–584.

Grevemeyer, I., Kaul, N., Diaz-Naveas, J.L., Villinger, H., Ranero, C.R. & Reichert, C., 2005. Heat flow and bending-related faulting at subduction trenches: case studies offshore of Nicaragua and Central Chile, *Earth planet. Sci. Lett.,* **236,** 238–248.

Grevemeyer, I., Ranero, C.R., Flueh, E., Kläschen, D. & Bialas, J., 2007. Passive and active seismological study of bending-related faulting and mantle serpentinization at the Middle America trench, *Earth planet. Sci. Lett.,* **258,** 528–542.

Harris, R.N., Fisher, A.T. & Chapman, D., 2004. Fluid flow through seamounts and implications for global mass fluxes, *Geology,* **32**(8), 725–728, doi:10.1130/G20387.1.

Hasegawa, A., Horiuchi, S. & Umino, N., 1994. Seismic structure of the northeastern Japan convergent margin: a synthesis, *J. geophys. Res.,* **99**(B11), 22 295–22 312.

Hess, H.H., 1964. Seismic anisotropy of the uppermost mantle under oceans, *Nature,* **203,** 629–631.

Hutnak, M. *et al.,* 2008. Large heat and fluid fluxes driven through mid-plate outcrops on ocean crust, *Nature Geosci.*, **1,** 611–614.

Ivandic, M., Grevemeyer, I., Berhorst, A., Flueh, E.R. & McIntosh, K., 2008. Impact of bending related faulting on the seismic properties of the incoming oceanic plate offshore of Nicaragua, *J. geophys. Res.,* **113,** B05410, doi:10.1029/2007JB005291.

Kanamori, H., 1971. Seismological evidence for lithospheric normal faulting—the Sanriku earthquake of 1933, *Phys. Earth planet. Inter.,* **4,** 289–300.

Keen, C. & Tramonti, C., 1970. A seismic refraction survey on mid-Atlantic ridge, *Geophys. J. R. astr. Soc.,* **20,** 473–491.

Kennett, B.L.N. & Orcutt, J.A., 1976. A comparison of travel time inversions for marine refraction profiles, *J. geophys. Res.,* **81,** 4061–4070.

Korenaga, J., Holbrook, W.S., Kent, G.M., Kelemen, P.B., Detrick, R.S., Larsen, H.-C., Hooper, J.R. & Dahl-Jensen, T., 2000. Crustal structure of the southeast Greenland margin from joint refraction and reflection seismic tomography, *J. geophys. Res.,* **105,** 21 591–21 614.

Korenaga, J., Keleman, P.B. & Holbrock, W.S., 2002. Methods for resolving the origin of large igneous provinces from crustal seismology, *J. geophys. Res.,* **107,** doi:10.1029/2001JB001030.

Langseth, M.G. & Silver, E.A., 1996. The Nicoya convergent margin: a region of exceptionally low heat flow, *Geophys. Res. Lett.,* **23,** 891–894.

Leeman, W.P., Carr, M.J. & Morris, J.D., 1994. Boron geochemistry of the Central American volcanic arc—constraints on the genesis of subduction-related magmas, *Geochim. cosmochim. Acta,* **58,** 149–168.

Lefeldt, M. & Grevemeyer, I., 2008. Centroid depth and mechanism of trench-outer rise earthquakes, *Geophy. J. Int.,* **172**(1), 240–251.

Lefeldt, M., Grevemeyer, I., Goßler, J. & Bialas, J., 2009. Intraplate seismicity and related mantle hydration at the Nicaraguan trench outer rise, *Geophys. J. Int.,* **178,** 742–752, doi:10.1111/j.1365-246X.2009.04167X

Morris, J., Leeman, W.P. & Tera, F., 1990. The subducted component in island arc lavas: constraints from Be isotopes and B–Be systematics, *Nature,* **344,** 31–36.

Moser, T.J., 1991. Shortest path calculation of seismic rays, *Geophysics,* **56,** 59–67.

Moser, T.J., Nolet, G. & Snieder, R., 1992. Ray bending revisited, *Bull. seism. Soc. Am.,* **82,** 259–288.

Osler, J.C. & Louden, K.E., 1995. The extinct spreading centre in Labrador Sea. I: crustal structure from a 2-D seismic refraction velocity model, *J. geophys. Res.,* **100,** 2261–2278.

Peacock, S.M., 2001. Are the lower planes of double seismic zones caused by serpentine dehydration in subducting oceanic mantle? *Geology,* **29,** 299–302.

Peacock, S.M., 2004. Insight into the hydrogeology and alteration of oceanic lithosphere based on subduction zones and arc volcanisms, in *Hydrogeology of Oceanic Lithosphere,* pp. 659–676, eds Davis, E.E & Elderfield, H., Cambridge University Press, New York.

Peacock, S.M., van Keken, P., Holloway, S.D., Hacker, B.R., Abers, G.A. & Fergason, R.L., 2005. Thermal structure of the Costa Rica–Nicaragua subduction zone, *Phys. Earth planet. Inter.,* **149,** 187–200.

Raitt, R.W., 1963. The crustal rocks, in *The Sea,* Vol. 3, pp. 85–102, ed. Hill, M.N., Interscience, New York.

Ranero, C.R., Phipps Morgan, J., McIntosh, K. & Reichert, C., 2003. Bending, faulting, and mantle serpentinization at the Middle America Trench, *Nature,* **425,** 367–373.

Ruepke, L., Phipps Morgan, J., Hort, M. & Connoly, J.A.D., 2002. Are the regional variations in Central American arc lavas due to differing basaltic peridotitic slab sources of fluids? *Geology,* **30,** 1035–1038.

Sallares, V., Charvis, P.H., Flueh, E.R. & Bialas, J., 2003. Seismic structure of Cocos and Malpelo ridges and implications for hotspot-ridge interaction, *J. geophys. Res.,* **108,** 2564, doi:10.1029/2003JB002431.

Schmitt, D.R., Han, Z., Kravchinsky, V. & Escartin, J., 2007. Seismic and magnetic anisotropy of serpentinized ophiolite: implications for oceanic spreading rate dependent anisotropy, *Earth planet. Sci. Lett.,* **261**(3–4), 590–601.

Silver, E., Kastner, M., Fisher, A., Morris, J., McIntosh, K. & Saffer, D., 2000. Fluid flow paths in the Middle America Trench and Costa Rica margin, *Geology,* **28**(8), 679–682.

Stein, C. & Stein, S., 1994. Constraints on hydrothermal flux through the oceanic lithosphere from global heat flow, *J. geophys. Res.,* **99,** 3081–3095.

Syracuse, E.M., Abers, G.A., Fischer, K., MacKenzie, L., Rychert, C., Protti, M., Gonzalez, V. & Strauch, W., 2008. Seismic tomography and earthquake locations in the Nicaraguan and Costa Rican upper mantle, *Geochem. Geophys. Geosyst.,* **9,** Q07S08, doi:10.1029/2008GC001963.

Tarantola, A., 1987. *Inverse Problem Theory: Methods for Data Fitting and Model Parameter Estimation,* 613 pp, Elsevier Sci., New York.

Tonarini, S., Agostini, S., Doglioni, C., Innocenti, F. & Manetti, P., 2007. Evidence for serpentinite fluid in convergent margin systems: the example of El Salvador (Central America) arc lavas, *Geochem. Geophys. Geosyst.,* **8,** Q09014, doi:10.1029/2006GC001508.

Toomey, D.R. & Foulger, G.R., 1989. Tomographic inversion of local earthquake data from the Hengill-Grensdalur central volcano complex, Iceland, *J. geophys. Res.,* **94,** 17 497–17 510.

Turner, S., McDermott, F., Hawkesworth, C. & Kepezhinskas, P., 1998. A U-series study of lavas from Kamchatka and the Aleutians: constraints on source composition and melt processes, *Contrib. Mineral. Petrol.,* **133,** 217–234.

Ulmer, P. & Trommsdorff, V., 1995. Serpentine stability to mantle depths and subduction-related magmatism, *Science,* **268,** 858–861.

White, R.S., McKenzie, D. & O'Nions, R.K., 1992. Oceanic crustal thickness from seismic measurements and rare earth element inversions, *J. geophys. Res.,* **97,** 19 683–19 715.

Whitmarsh, R.B., 1978. Seismic refraction studies of the upper igneous crust in the North Atlantic and porosity estimates for layer 2, *Earth plant. Sci. Lett.,* **37,** 451–464.

Wilson, D.S. *et al.,* 2003. *Proceedings of the Ocean Drilling Program, Initial Reports,* Vol. 206, Ocean Drilling Program, College Station, TX, doi:10.2973/odp.proc.ir.206.2003.